

JammingSnake: A follow-the-leader continuum robot with variable stiffness based on fiber jamming

Chen Qian, *Student Member, IEEE*, Tangyou Liu, *Student Member, IEEE*, and Liao Wu*, *Member, IEEE*

Abstract—Follow-the-leader (FTL) motion is essential for continuum robots operating in fragile and confined environments. It allows the robot to exert minimal force on its surroundings, reducing the risk of damage. This paper presents a novel design of a snake-like robot capable of achieving FTL motion by integrating fiber jamming modules (FJMs). The proposed robot can dynamically adjust its stiffness during propagation and interaction with the environment. An algorithm is developed to independently control the tendon and FJM insertion movements, allowing the robot to maintain its shape while minimizing the forces exerted on surrounding structures. To validate the proposed design, comparative tests were conducted between a traditional tendon-driven robot and the novel design under different configurations. The results demonstrate that our design relies significantly less on contact with the surroundings to maintain its shape. This highlights its potential for safer and more effective operations in delicate environments, such as minimally invasive surgery (MIS) or industrial in-situ inspection. A video demonstration of performance test on *JammingSnake* can be found at <https://youtu.be/P2YTCPWHNfo>.

Index Terms—Follow-the-leader, Stiffness variation, Continuum robot, Fiber jamming.

I. INTRODUCTION

Follow-the-leader (FTL) motion is essential for continuum robots propagating in confined or sensitive environments, as it ensures that the robot body follows the same path traced by its leading section. This minimizes the risk of collision and damage to surrounding structures, which is especially important in delicate operations like minimally invasive surgery or industrial inspection of narrow passages [1]–[3]. The FTL approach allows for precise movement, maintaining low deviation from the desired trajectory, and quick adaptation to environmental changes.

Different approaches have been proposed to address the FTL problem. One group of methods is through algorithmic approximation. For instance, tendon-driven continuum robots (TDCRs) with multiple sections can approximate FTL by controlling the bending angle of each section following elaborately designed strategies [4]. However, such designs introduce errors during FTL motion propagation, particularly for trajectories that contain non-constant curvature segments. Additionally, the fixed length of each section and its ability to bend in only one degree of freedom prevent the design from continuously

adapting its shape during propagation to meet the requirements of precise FTL motion [5].

Acknowledging the shortcomings of algorithmic approximation, another group of approaches aims to achieve “true” FTL motion through innovative hardware designs. For example, concentric tube continuum robots (CTCRs), which are composed of pre-curved, flexible tubes nested within one another, are capable of FTL motion [6]. By rotating and translating the tubes separately, the robot’s tip follows a defined trajectory, with the body mirroring the same path. This continuous curvature control ensures precise motion along narrow or complex pathways. However, the pre-bent shapes of the tubes limit the range of operation as the robot’s motion is constrained by the fixed curvature of the tubes, reducing adaptability to trajectories outside the predefined curvature. [7].

To allow a wider operational range, one popular method is to introduce variable stiffness modules [8]. Such a design usually consists of multiple components that can transition between soft and rigid phases [9], [10]. By steering and propagating the robot in the soft phase and conserving the path’s shape in the rigid phase, the robot can potentially enable FTL [11].

One of the early attempts was the Highly Articulated Robotic Probe (HARP) proposed by Degani et al [11]. This design includes a pair of continuum robots assembled concentrically, and each pair can alter its stiffness separately by changing the tendon-pulling force to trigger segment locking. However, a notable disadvantage of this design is that both stiffness variation and robot steering are controlled using the same tendon-pulling mechanism. As a result, applying a pulling force to lock the segments often inadvertently induces unintended bending of the robot. This coupling effect complicates operation, leads to deviations from the desired posture and increases the risk of operational errors in complex environments. Since actuation needs to occur at the robot’s proximal end, maintaining stiffness with HARP becomes more challenging as the robot length increases, particularly when used as an end effector for a long passive endoscope. Moreover, the contact area between the two segments must be large enough to maintain sufficient frictional force, limiting the robot’s flexibility in bending.

More recent designs aimed to focus the tendon locking specifically on robot control while incorporating new mechanisms to enable variations in stiffness, such as probe clamp triggered by Shape Memory Alloy (SMA) [12]–[14]. Such designs eliminate the coupling issue and hence reduce operation errors. However, the complexity of the clamp prevents the robot from being downsized to less than 30 mm in diameter. Moreover, the response time of SMA is typically

This work was supported by the Australian Research Council under Grant DP250102489.

*Corresponding author: Liao Wu, dr.liao.wu@ieee.org.

C. Qian, T. Liu, and L. Wu are with the School of Mechanical and Manufacturing Engineering, University of New South Wales, Sydney, NSW 2052, Australia.

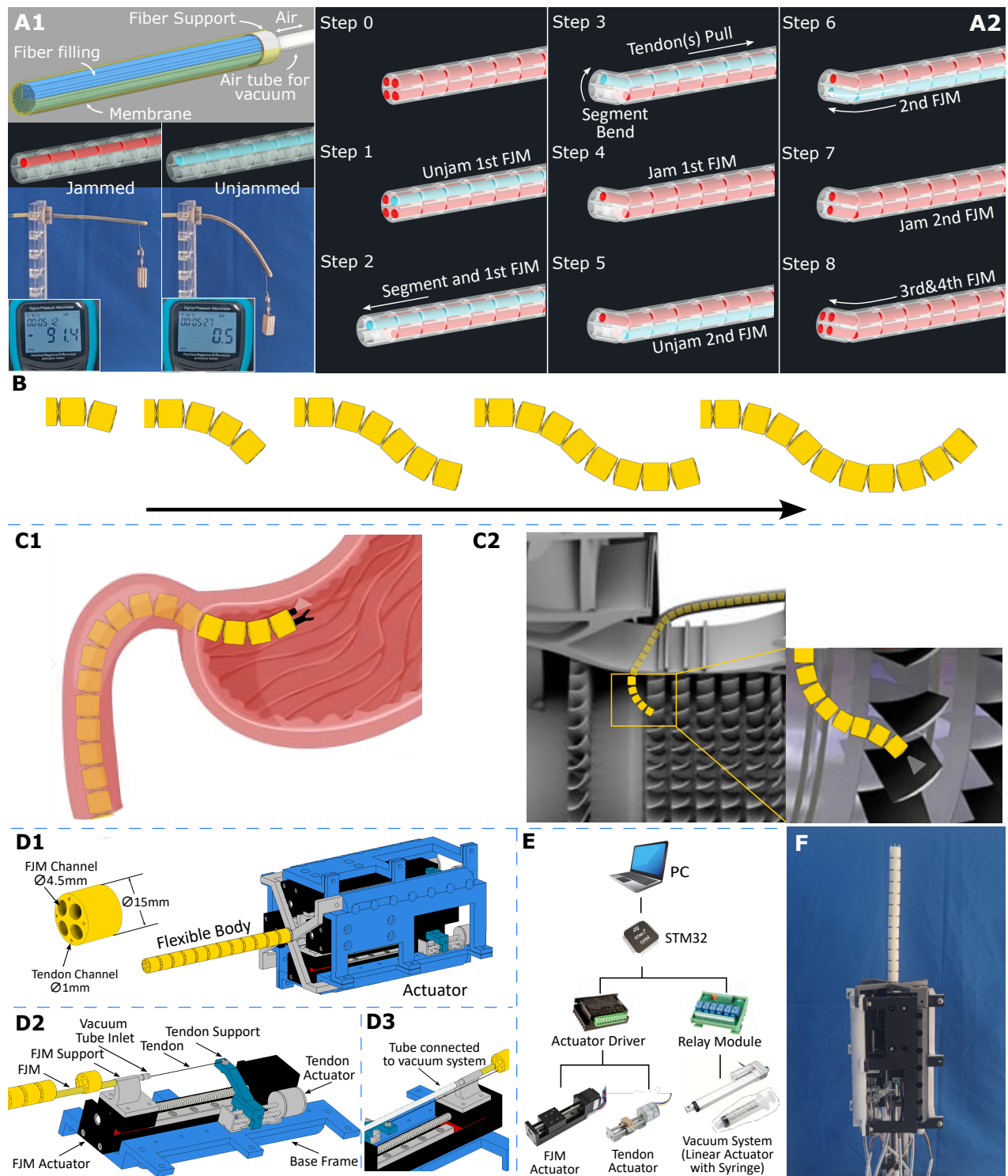


Fig. 1. (A1): A Fiber Jamming Module (FJM) is a soft robotic component consisting of fibers within an elastic membrane, capable of achieving rapid and significant stiffness variation through air vacuuming. Photos illustrate the stiffness of an FJM under two conditions: when vacuumed at -90 kPa and when not vacuumed. (A2): An illustrative demonstration of a complete cycle of our prototype shows the transition from one preserved shape to the next. The procedural details of the FTL mechanism are as follows: **Step 0**: Initially, all FJMs are jammed to preserve the flexible body's shape. **Step 1**: Unjam the first FJM. **Step 2**: Propagate the robot segments with the unjammed FJM. **Step 3**: Engage the tendon(s) to steer the head segment to the target orientation. **Step 4**: Jam the propagated FJM to conserve the flexible body's new shape. **Step 5**: Unjam the second FJM. **Step 6**: Extend the unjammed FJM to the same length as the first. **Step 7**: Jam this FJM to stabilize the robot in its updated configuration. **Step 8**: Repeat Steps 5-7 for the third and fourth FJMs. The flexible body is now in a new stable position (as in Step 0) and ready for the next cycle. (B) An illustration demonstrates how FTL motion is facilitated by repeating the cycle in (A). (C) Two potential applications for our prototype, which require the flexible body to travel through narrow channels to reach open spaces: medical surgery and engine in-situ inspection. (D) Illustration of prototype design, including the flexible body and actuator system. (D2) The actuator section is composed of four identical parts, each equipped with individual actuators to control the pulling force of the tendons and the movement of the FJMs. (D3) The back view displays the configuration of the tendons and vacuum tube. (E) Illustration of the control system setup. (F) The photo of the robot prototype.

10 seconds or more. This delayed responsiveness restricts its effectiveness in dynamic environments where rapid actuation or quick adaptation is required, posing a significant barrier to its broader use in real-time robotic systems.

Similarly, attempts involving Low Melting Point Alloy (LMPA) [15] have also faced difficulties in practical applications due to the slow response time of the material. The heating time for LMPA is typically 15 seconds, and the cooling time is around 30 seconds.

Jamming modules show advantages in responding time [16], shape adaptability [17], and structural simplicity [13], [14], highlighting their unexplored potential in FTL applications [2]. A jamming module usually comprises a sealed soft membrane and fillings inside (Fig. 1A1). When no pressure is applied, the module exhibits soft properties, whereas when high vacuum pressure is applied, fillings are jammed. The module hence becomes rigid due to the increased friction force between the filling [18]. Based on the geometry of the filling, jamming modules can be classified into three types: granular, fiber, and layer jamming. There was preliminary work to implement granular jamming into a snake-like robot [19]. However, no one has considered fiber jamming, which is particularly suited for continuum robots due to its capability to restrict longitudinal shape changes while permitting flexibility in other directions, making it an ideal choice for such applications.

In our previous paper [20], we conducted a theoretical and experimental study on fiber jamming modules (FJMs) for stiffness variation. To evaluate their integration in slender robots, we designed and fabricated FJMs with an inner diameter of 4mm. The experimental results identify the optimal configurations needed to achieve the desired characteristics. These findings support the feasibility of integrating small-sized FJMs, while other factors, such as fiber bundle arrangement and geometry studied in previous research, may not be as relevant.

To demonstrate the strong potential of FJMs to achieve FTL motion when integrated into a continuum robot, we propose the *JammingSnake*: a novel design that enables FTL motion without the need for complex control algorithms. The prototype also proves to be a promising end effector for an endoscope, addressing stiffness variation issues when actuation occurs at the proximal end as the endoscope length increases. Additionally, we see strong applicability for this prototype in confined space operations, such as medical endoscopy and engine in-situ inspection.

II. PROTOTYPE DESIGN

JammingSnake contains three main components: the robot, the actuator, and the control system (Fig. 1D). The robot consists of 12 segments, each measuring 15 mm in diameter and 15 mm in length, for a total length of 180 mm. Each segment has four tendon channels and four FJM channels. The tendon channels are in 1 mm diameter and the FJM channels are in 4.5 mm diameter.

A. Design Concept

To enable FTL motion without reliance on environmental constraints, the continuum robot must perform three essential

sub-functions: **conservation, steering, and propagation** [2]. These sub-functions are managed through alternating states in which multiple FJMs integrated within the prototype are jammed or unjammed. By controlling the stiffness of each FJM, the flexible body of the robot can dynamically adjust its structure to conserve shape, steer toward a designated trajectory, and progress forward. This method allows for precise and adaptable motion, enhancing the robot's functionality in diverse, unstructured environments.

Fig. 1A2 illustrates one full cycle of the FTL mechanism in *JammingSnake*: robot segments with unjammed (soft) FJMs facilitate steering and propagation along a trajectory maintained by jammed (rigid) FJMs. By repeating the cycle, our robot can achieve FTL without relying on the surrounding environment (Fig. 1B). It is noted that, while two FJMs can achieve the FTL mechanism, our prototype incorporates four FJMs to enhance structural stability and functionality. In actual operation, the prototype can complete the FTL motion with more than one segment extended in a cycle, depending on the desired shape and complexity of the path trajectory. This flexibility allows the robot to adapt its configuration to navigate intricate paths more effectively.

Additionally, since a minimum of two FJMs is sufficient to achieve FTL motion, the number of FJMs in the prototype can be reduced based on the operational payload. The spare FJMs can either be employed to enhance the stiffness of specific sections of the robot or replaced with alternative components for specialized tasks. This adaptability optimizes the robot's performance while allowing for efficient resource utilization.

B. Application

We designed this robot with specific scenarios in mind, aiming to make it highly effective for applications that involve navigating through constrained pathways and achieving precise maneuverability. In these scenarios, the robot must first traverse a long, narrow channel and then enter a larger open space. Once in the open area, the robot needs to independently reach its target without relying on nearby surfaces for support.

To achieve this, our robot is designed to extend the length of its flexible body, ensuring precision and flexibility while minimizing reliance on complex support mechanisms. FTL motion is particularly crucial in scenarios requiring high agility and stability within large or expansive areas.

This type of working scenario has potential applications in fields like medical procedures [21]–[23] and industrial inspection [24]. For example, in gastric surgery, an endoscope must navigate through the recta to reach the stomach before performing precise operations within the larger cavity (Fig. 1C1). Similarly, a borescope used for in-situ inspection, such as checking components within a compressor (Fig. 1C2), benefits greatly from the FTL motion and dexterity of this robotic design. These capabilities ensure both precise targeting and ease of control in environments where traditional robotic systems may face significant limitations.

C. Actuator Design

The actuator system is approximately 220 mm long, 120 mm wide, and 120 mm high, consisting of four identical

parts arranged in a circular configuration, each positioned at 90° (Fig. 1D2). Each part includes a base frame that supports a 20 mm stepper motor for tendon pulling and a 28 mm stepper motor for FJM movement. The tendon stepper motors are controlled to bend the head segment (Step 3 in Fig. 1A2), while the FJM stepper motors independently control the insertion or retreat of the FJMs into the flexible body, enabling the desired FTL motion (Step 6).

A 40 mm base stepper motor is integrated into the actuator to perform the insertion of the entire robot. The speed of this motor is synchronized with that of the FJM stepper motors. Consequently, as the base stepper motor advances the robot and the FJM stepper motors retract the FJMs at the same speed, and the flexible body appears to propagate forward without altering the insertion depth of the FJMs, as illustrated in Step 2. This motor serves as the proximal section of the robot and can be replaced by other actuators, such as a robotic arm, in actual applications.

D. Control System

As shown in Fig. 1E, the control system is powered by a 24 V supply that drives the stepper motor controllers, managing the FJMs, tendons, and actuator. A 50 ml syringe, connected to the linear actuator, serves as a pump to generate a vacuum within the FJM. Each linear actuator is equipped with a relay module that enables bidirectional control, allowing the syringe to alternate between vacuuming and releasing the FJMs as needed. All signals within the system are managed by an STM32 microcontroller board, which communicates with a computer for manual and routine control. This allows precise coordination and control of the various components to ensure smooth operation and adaptability to different tasks.

III. KINETIC MODEL

In our prototype, tendons are used solely to bend the tip, allowing this actuation method to be easily replaced for future applications. During other phases, the tendons remain loose to avoid obstructing shape preservation. Precise length adjustments for both tendons and FJMs are essential, based on the steering angle and joint dimensions, to ensure optimal shape conservation [25]–[27].

Fig. 2 illustrates the model used to describe the length variations of tendons and FJMs between two robot segments, accounting for a bending angle of $\Delta\theta$ and the twist offset of $\Delta\gamma$. Considering that the channel outlets for tendons and FJMs are located at different layers within the robot segment (Fig. 2B), the adjustable lengths of the tendons and FJM (Fig. 2C) can be expressed as:

$$l(\Delta\theta, \Delta\gamma, \psi) = 2r \left(1 - \frac{\cos \psi}{\cos \phi} \cos \left(\phi - \frac{\Delta\theta}{2} \right) \right)$$

where $\phi = \tan^{-1}(\tan \psi \cdot \cos \Delta\gamma)$

$$\psi = \begin{cases} \alpha & \text{for tendon} \\ \beta & \text{for FJM} \end{cases} \quad (1)$$

The FJM diameter is too large to be treated as a wire, so its movement is approximated based on the centerline of the

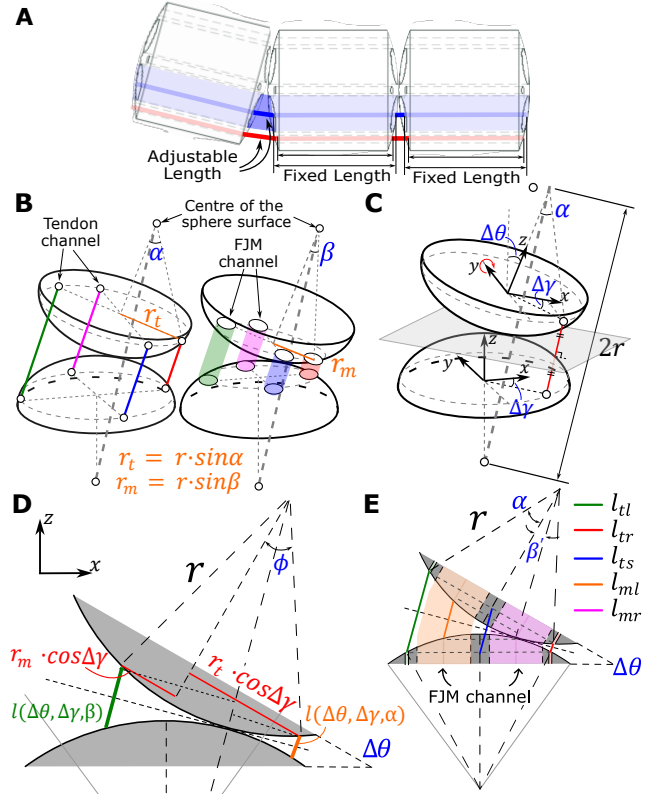


Fig. 2. An illustration details the calculation of adjusted FJM and tendon lengths: (A) Tendon and FJM lengths within each segment are fixed, with adjustable lengths referring between the channel outlets of adjacent segments. (B) Robot joint model showing tendon and FJM channel positions, where angles α and β represent their positions relative to the sphere's surface symmetry axis. (C) Length calculation with a bending degree of $\Delta\theta$ and a twist offset of $\Delta\gamma$ at the tip segment. (D) Cross-sectional view in the x-z plane (E) Diagram showing the length of tendon and FJM when $\Delta\gamma = 0$, where l_{tl} : left tendon; l_{tr} : right tendon; l_{ts} : side tendon; l_{ml} : left FJM; l_{mr} : right FJM.

FJM channels. During prototype testing, we simplified the adjusted lengths of tendons and FJMs by setting the right tendon channel to $\Delta\gamma = 0$:

$$\begin{aligned} l_{tl} &= l(\Delta\theta, \pi, \alpha) = 2r \left(1 - \cos \left(\alpha + \frac{\Delta\theta}{2} \right) \right) \\ l_{tr} &= l(\Delta\theta, 0, \alpha) = 2r \left(1 - \cos \left(\alpha - \frac{\Delta\theta}{2} \right) \right) \\ l_{ts} &= l(\Delta\theta, \frac{\pi}{2}, \alpha) = 2r \left(1 - \cos \alpha \cdot \cos \frac{\Delta\theta}{2} \right) \\ l_{ml} &= l(\Delta\theta, \frac{\pi}{4}, \beta) = 2r \left(1 - \frac{\cos \beta}{\cos \beta'} \cos \left(\beta' + \frac{\Delta\theta}{2} \right) \right) \\ l_{mr} &= l(\Delta\theta, \frac{3\pi}{4}, \beta) = 2r \left(1 - \frac{\cos \beta}{\cos \beta'} \cos \left(\beta' - \frac{\Delta\theta}{2} \right) \right) \end{aligned} \quad (2)$$

where $\beta' = \tan^{-1}(1/\sqrt{2}\cos\beta)$

These calculations help us regulate the tendon pulling force during prototype propagation, preventing the tendon from being overloaded or over-tensioned. Additionally, it enhances the precision of positioning the FJMs relative to the robot segments, which is critical for achieving the best FTL motion.

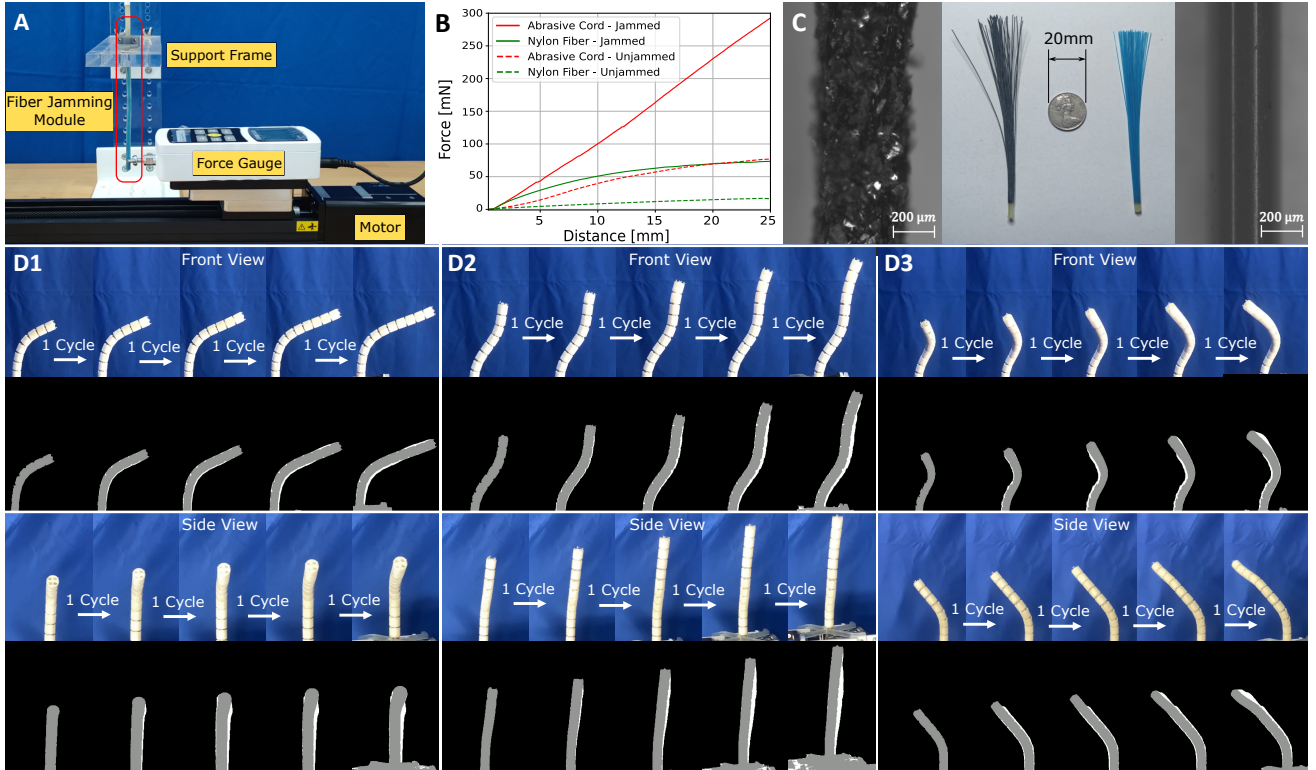


Fig. 3. (A) The stiffness test setup used a force gauge to measure the FJM’s resistance force and a stepper motor to record displacement. (B) Results show that FJMs with abrasive cords have higher, more linear stiffness than nylon fiber bundles in both jammed and unjammed states. (C) Images at 50x magnification show that abrasive cords have rougher surfaces than nylon fibers, reducing slippage and increasing jammed stiffness. (D) An illustration shows how the prototype maintains its shape while propagating in C shape (D1), S shape (D2) and spiral shape (D3) configurations. Tests indicate that jammed FJMs with abrasive cords effectively retain the robot’s shape as its segments propagate.

IV. PERFORMANCE TEST

A. Shape Conservation Performance

A preliminary test was conducted to evaluate the updated FJM with abrasive cords for shape conservation and to assess its performance during propagation. The FJMs were jammed as the robot segments advanced.

In our prior research [20], we determined the optimal configuration for the number and density of fibers in FJMs with an inner diameter of 4 mm, using 0.4 mm fibers at a packing density of 56%, resulting in a stiffness variation of up to 3400%. Further improvements in this work involved replacing nylon fibers with abrasive cords to enhance overall stiffness, building on insights from previous studies [28]. Tests confirm that FJMs with abrasive cords demonstrate a stiffness variation ratio comparable to that of nylon fibers while offering increased overall rigidity (Fig. 3A&B). Moreover, high-magnification microscopy (50x) revealed the abrasive cords’ rough surface texture, which enables a more linear jamming response and enhances stability during robot propagation (Fig. 3C).

To assess the accuracy of the shape conservation behavior of our prototype, we employed a sweeping-area method to visualize the error, referencing the work of Grassmann et al. [5]. A custom script processed video footage of the robot’s propagation, categorizing it into three colors: black for the background, grey for the robot, and white for the area traversed by the robot. This approach provided a clear visualization of the robot’s movement and spatial occupancy.

As shown in Fig. 3D, the video analysis results indicated very limited white area, suggesting that our prototype demonstrates exceptional performance in maintaining shape conservation while propagating. This finding reinforces the effectiveness of the updated FJM with abrasive cords in achieving the desired operational characteristics in robotic applications. This stability is crucial for retaining the robot’s configuration along complex paths, ensuring consistent positioning in demanding environments.

B. Force Exertion Performance

JammingSnake highlights minimal force exertion on surrounding structures as a key innovation achieved through FJMs. To evaluate its effectiveness, we developed a testing methodology that simulates narrow paths, allowing us to assess the robot’s performance in constrained environments.

In our robot segment design, the standard bending angle between two segments is set to 10°, where the segments make contact at the center of their top surfaces. This gentle bend minimizes the offset in the FJM channels, allowing the FJMs to pass through smoothly during propagation.

For sharper bending, the bending angle can reach up to 15°, bringing the segments into contact at the closer tendon channels. While the FJMs can still pass through at this angle, the increased offset introduces additional friction due to the movement of the FJMs. This added friction can result in greater deformation of the robot from its conserved shape and,

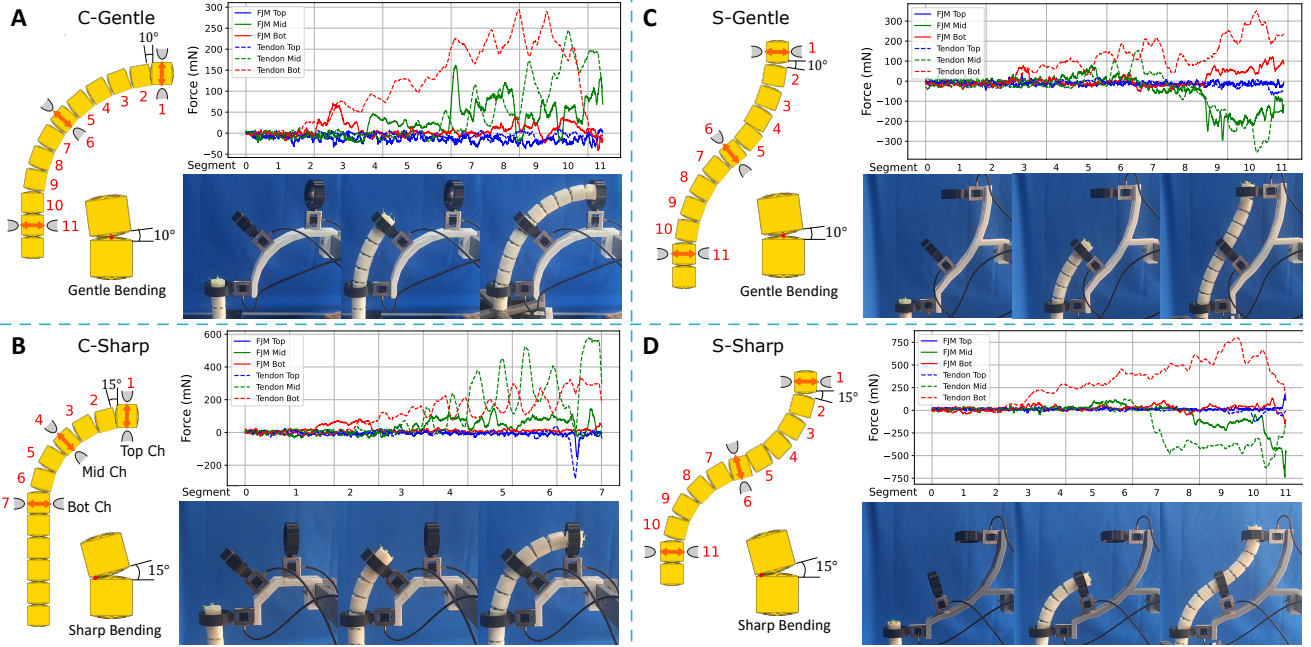


Fig. 4. The test included two bending scenarios: gentle bending (10° angle between two adjacent segments) and sharp bending (15° between two adjacent segments, the robot's maximum bending angle). For each scenario, the robot performed one-section (C shape) and two-section (S shape) bending to evaluate shape conservation. Force sensors at three checkpoints (bottom, middle, and top of the trajectory) measured forces exerted by the robot. The graphs compare force responses for TDCR and FJM-assisted operations, showing significantly lower forces exerted by FJM-assisted operation across all scenarios.

TABLE I
SUMMARY OF FORCE EXERTED BY THE ROBOT TO THE CHECKPOINTS

Testing Scenarios	Checkpoint	Max Force Exertion - Phase I		Max Force Exertion - Phase II		Max Force Exertion - Phase III	
		Tendon only	FJM assisted	Tendon only	FJM assisted	Tendon only	FJM assisted
C-Gentle	Bottom	105mN	No touch	232mN	No touch	55mN	No touch
	Middle	-	-	139mN	78mN	175mN	72mN
	Top	-	-	-	-	No touch	No touch
C-Sharp	Bottom	70mN	No touch	189mN	73mN	254mN	52mN
	Middle	-	-	296mN	No touch	338mN	No touch
	Top	-	-	-	-	38mN	No touch
S-Gentle	Bottom	84mN	No touch	236mN	51mN	262mN	80mN
	Middle	-	-	205mN	108mN	242mN	147mN
	Top	-	-	-	-	31mN	No touch
S-Sharp	Bottom	268mN	No touch	682mN	40mN	463mN	No touch
	Middle	-	-	401mN	137mN	420mN	307mN
	Top	-	-	-	-	40mN	26mN

* Table represents the maximum of the average values for each segment after completing the entire pass process at three designated checkpoints.

in confined areas, can lead to increased force exerted on the surrounding environment. Therefore, sharp bending is tested as an extreme scenario to quantify the maximum force the robot is expected to exert on its surroundings.

The testing procedure began by setting up a controlled environment with defined narrow pathways to simulate real-world constraints. During the tests, we set up three checkpoints at the beginning, middle, and end of the pathway. The inner diameter of the checkpoints is 20 mm, while the outer diameter of the prototype robot is 15 mm. A single-axis force sensor is installed at each checkpoint to record the forces exerted by the robot on its surroundings as it propagates through these pathways. This allowed us to assess the interaction between the robot and its environment, providing valuable data on the forces involved in maintaining shape and stability.

The two most common scenarios in real-life operation, single-section bending (C shape) and two-section bending

(S shape) were tested under both gentle and sharp bending conditions. The entire propagation process was divided into three phases based on the tip position:

- Phase I: The tip passes the bottom checkpoint;
- Phase II: The tip crosses the middle checkpoint;
- Phase III: The tip reaches the top checkpoint and continues until the process is complete.

The exerted force at each of the three checkpoints was calculated as the mean force applied by each individual segment over the full duration of the passing process. The highest mean force recorded during each phase at each checkpoint was used as a benchmark for analysis to assess the prototype's shape conservation performance.

For comparative analysis, we repeated the same tests on the prototype without activating the FJMs, allowing it to function as a standard Tendon-Driven Continuum Robot (TDCR). By examining the differences in force exertion between the two

TABLE II
COMPARISON WITH FOLLOW THE LEADER CONTINUUM ROBOT BASED ON STIFFNESS VARIATION MECHANISMS

Ref	OD [mm]	Length [mm]	Stiffness Variation Type	Max Bending Range [°]	Actuation Time of Stiffness Variation [s]	Coupling between steering and stiffness variation
This work	15	180	Fiber jamming	180	2s	Decoupled
[5], [29]	7	165	Actuated segment	180	N/A*	Coupled
[11]	12	300	Segment locking by tendon	15 per segment	≈1s*	Coupled
[30]	12	80	SMP	127	14 / 64 (heating/cooling)	Decoupled
[15]	21	150	LMPA	N/A*	15 / 30 (heating/cooling)	Decoupled
[12]	30	≈240*	Rod clamping	180	10-11	Decoupled

* Some data in the table for previous designs were not explicitly provided in their respective papers; these values were estimated based on available illustrations and demonstration videos, or labelled as “N/A” in the table.

configurations, we aimed to quantify the advantages offered by the FJMs in terms of shape conservation and overall performance.

Fig. 4 presents photos of the prototype progressing through the three phases, along with the raw force reading data. The processed data are summarized in Table. I. The result illustrates a notable difference in the forces exerted by the FJM-assisted robot segments compared to the Tendon-only setup across different bending configurations (C shape and S shape). The data indicates that the FJM-assisted robot maintains lower forces on surrounding surfaces, especially in configurations that involve sharper turns or more complex paths.

A noteworthy result is that our prototype exerts significantly less force on the surroundings than a standard TDCR of the same diameter. This effect is especially pronounced in C shaped pathways, which are relatively simple to navigate. Whether in a sharp or gentle C shape configuration, our prototype did not apply any force to the bottom checkpoint before entering Phase II and exerted less than 80 mN on the surrounding force sensor throughout the entire propagation.

In contrast, the non-FJM-assisted robot exerted up to 338 mN at the middle checkpoint and 254 mN at the bottom checkpoint. Consequently, in real-world scenarios where pathways are confined, it can be predicted that nearly the entire pathway, except the area near the final target position, will experience significantly higher forces.

A similar situation was also observed in the S shape configurations with distinct advantages emerging for the FJM approach. In the S-Gentle configuration, the FJM-assisted robot consistently exerts lower forces at all checkpoints, with values at up to 147 mN at the checkpoints compared to the force at a maximum of 262 mN in the Tendon-only setup. The same trend is observed in the S-Sharp configuration, where the FJM-assisted robot demonstrates significantly lower force exertion, recording only 137 mN at the middle checkpoint versus 401 mN in the Tendon-only setup.

In configurations like C-Sharp and S-Sharp, increased friction from tendon-only bending raises force requirements to maintain trajectory. However, the FJM-assisted robot adjusts its rigidity to environmental constraints, enabling smoother transitions. For instance, at the C-Sharp bottom checkpoint in Phase I, the FJM-assisted robot showed “No touch”, exerting zero force, compared to 70 mN in the tendon-only setup.

V. DISCUSSION

Table. II compares our prototype with multiple existing continuum robot designs that also achieve FTL motion through stiffness variation mechanisms. Based on the table comparison, *JammingSnake* shows balanced merits across various aspects. Here are the key points highlighting why our prototype is either better or at least highly competitive as a novel design:

- 1) **Compact Size:** With an outer diameter (OD) of 15 mm and a length of 180 mm, our design is both compact and appropriately sized for many constrained environments where continuum robots must operate, from medical to industrial applications. Other designs vary significantly in size; for example, the rod clamping mechanism [12] has a much larger OD of 30 mm, which may limit its applications in narrow or delicate environments.
- 2) **Reasonable Actuation Time of Stiffness Variation:** Our prototype achieves a fast actuation time of 2 seconds, which is significantly competitive. Some other designs, like those using SMP [30] and LMPA [15], have actuation times that can be much slower. Our faster response time can be critical for applications that demand real-time adjustments where delays could impact efficiency and safety. In addition, the current actuation time is limited by the actuator, not the mechanism, making it easier to be reduced.
- 3) **Error Resilience Over Long Distances:** Our prototype employs a decoupled control mechanism, avoiding the length-dependent errors seen in other designs. Coupled control systems, which link robot movement and stiffness variation through shared actuation like tendon-pulling, often cause unintended interactions—such as unintentional bending during stiffness adjustments or disrupted stiffness during bending. These interactions complicate precise control, increasing operational errors, especially in tasks requiring the robot as an end effector. For example, several designs (e.g., [5], [11], [29]) exhibit length-dependent errors, limiting their effectiveness as end-effectors over longer distances. Our prototype, with its decoupled mechanism, ensures consistent performance and accuracy regardless of the robot’s length.

Overall, our prototype achieves a competitive balance of compact size, efficient actuation, and exceptional error resilience over distance. Its fiber jamming mechanism delivers a broad, continuous range of stiffness control, enhancing its robustness and suitability for FTL continuum robots. These

features make it highly promising for applications requiring precision, adaptability, and reliable performance in confined or hard-to-access environments.

Although our current prototype has a 15 mm diameter, it could be reduced to 10 mm with smaller FJMs or improved configurations of FJM channels, enhancing compatibility with narrow surgical or industrial inspection channels. In addition, by replacing the current pump system with a bidirectional pump system, we can easily reduce the time of stiffness variation actuation to less than 1 second, which can be compatible with other designs.

VI. CONCLUSION

In conclusion, we have developed *JammingSnake*, a continuum robot capable of achieving FTL motion through the use of FJMs, providing significant advantages over existing designs. This approach introduces a unique mechanism where FJMs, capable of transitioning between flexible and rigid states, allow the robot to conserve its shape and adaptively stiffen specific sections as needed. Through this design, we have demonstrated significantly reduced force exertion on surrounding structures compared to traditional TDCRs, highlighting the advantages of FJMs in minimizing friction and improving stability in narrow, confined spaces. Additionally, our design supports precise shape control and minimizes manipulation error across extended distances from the actuator, making it particularly suitable for applications as an end effector in medical and industrial scenarios. Our proposed modifications, including optimized actuation and control systems, lay the groundwork for enhancing the robot's efficiency, adaptability and maneuverability in complex operational environments.

REFERENCES

- [1] H. Choset and W. Henning, "A follow-the-leader approach to serpentine robot motion planning," *Journal of Aerospace Engineering*, vol. 12, no. 2, pp. 65–73, 1999.
- [2] C. Culmone, S. F. Yikilmaz, F. Trauzettel, and P. Breedveld, "Follow-the-leader mechanisms in medical devices: A review on scientific and patent literature," *IEEE Reviews in Biomedical Engineering*, 2021.
- [3] Z. Li, L. Wu, H. Ren, and H. Yu, "Kinematic comparison of surgical tendon-driven manipulators and concentric tube manipulators," *Mechanism and Machine Theory*, vol. 107, pp. 148–165, 2017.
- [4] Y. Gao, K. Takagi, T. Kato, N. Shono, and N. Hata, "Continuum robot with follow-the-leader motion for endoscopic third ventriculostomy and tumor biopsy," *IEEE Transactions on Biomedical Engineering*, vol. 67, no. 2, pp. 379–390, 2019.
- [5] R. M. Grassmann, P. Rao, Q. Peyron, and J. Burgner-Kahrs, "Fas—a fully actuated segment for tendon-driven continuum robots," *Frontiers in Robotics and AI*, vol. 9, p. 873446, 2022.
- [6] H. B. Gilbert, J. Neimat, and R. J. Webster, "Concentric tube robots as steerable needles: Achieving follow-the-leader deployment," *IEEE Transactions on Robotics*, vol. 31, no. 2, pp. 246–258, 2015.
- [7] C. Bergeles, A. H. Gosline, N. V. Vasilyev, P. J. Codd, P. J. Del Nido, and P. E. Dupont, "Concentric tube robot design and optimization based on task and anatomical constraints," *IEEE Transactions on Robotics*, vol. 31, no. 1, pp. 67–84, 2015.
- [8] Y. Zhong, R. Du, L. Wu, and H. Yu, "A novel articulated soft robot capable of variable stiffness through bistable structure," in *2020 IEEE International Conference on Robotics and Automation (ICRA)*. IEEE, 2020, pp. 2939–2945.
- [9] M. Manti, V. Cacucciolo, and M. Cianchetti, "Stiffening in soft robotics: A review of the state of the art," *IEEE Robotics & Automation Magazine*, vol. 23, no. 3, pp. 93–106, 2016.
- [10] Z. Shang, J. Ma, and S. Wang, "Review of variable stiffness mechanisms in minimally invasive surgical manipulators," *Journal of Mechanical Engineering*, vol. 58, 07 2022.
- [11] A. Degani, H. Choset, A. Wolf, and M. A. Zenati, "Highly articulated robotic probe for minimally invasive surgery," in *Proceedings 2006 IEEE International Conference on Robotics and Automation, 2006. ICRA 2006*. IEEE, 2006, pp. 4167–4172.
- [12] B. Kang, R. Kojcev, and E. Sinibaldi, "The first interlaced continuum robot, devised to intrinsically follow the leader," *PLoS one*, vol. 11, no. 2, p. e0150278, 2016.
- [13] C. Yang, S. Geng, I. Walker, D. T. Branson, J. Liu, J. S. Dai, and R. Kang, "Geometric constraint-based modeling and analysis of a novel continuum robot with shape memory alloy initiated stiffness," *The International Journal of Robotics Research*, vol. 39, no. 14, pp. 1620–1634, 2020.
- [14] P. Wang, S. Guo, X. Wang, and Y. Wu, "Design and analysis of a novel variable stiffness continuum robot with built-in winding-styled ropes," *IEEE Robotics and Automation Letters*, vol. 7, no. 3, pp. 6375–6382, 2022.
- [15] Z. Xing, F. Wang, Y. Ji, D. McCoul, X. Wang, and J. Zhao, "A structure for fast stiffness-variation and omnidirectional-steering continuum manipulator," *IEEE Robotics and Automation Letters*, vol. 6, no. 2, pp. 755–762, 2020.
- [16] J. Wang, S. Wang, J. Li, X. Ren, and R. M. Briggs, "Development of a novel robotic platform with controllable stiffness manipulation arms for laparoscopic single-site surgery (less)," *The International Journal of Medical Robotics and Computer Assisted Surgery*, vol. 14, no. 1, p. e1838, 2018.
- [17] C. Li, X. Gu, X. Xiao, C. M. Lim, and H. Ren, "Flexible robot with variable stiffness in transoral surgery," *IEEE/ASME Transactions on Mechatronics*, vol. 25, no. 1, pp. 1–10, 2019.
- [18] S. G. Fitzgerald, G. W. Delaney, and D. Howard, "A review of jamming actuation in soft robotics," in *Actuators*, vol. 9, no. 4. MDPI, 2020, p. 104.
- [19] A. Jiang, P. Dasgupta, K. Althoefer, and T. Nanayakkara, "Robotic granular jamming: A new variable stiffness mechanism," *Journal of the Robotics Society of Japan*, vol. 32, no. 4, pp. 333–338, 2014.
- [20] C. Qian, T. Liu, and L. Wu, "Effects of fiber number and density on fiber jamming: Towards follow-the-leader deployment of a continuum robot," in *2024 IEEE/RSJ International Conference on Intelligent Robots and Systems (IROS)*. IEEE, 2024, pp. 9235–9240.
- [21] T. Liu, J. Wang, S. Wong, A. Razjigaev, S. Beier, S. Peng, T. N. Do, S. Song, D. Chu, C. H. Wang *et al.*, "A review on the form and complexity of human–robot interaction in the evolution of autonomous surgery," *Advanced Intelligent Systems*, vol. 6, no. 11, p. 2400197, 2024.
- [22] A. Razjigaev, A. Pandey, D. Howard, J. Roberts, A. Jaiprakash, R. Crawford, and L. Wu, "Optimal vision-based orientation steering control for a 3-d printed dexterous snake-like manipulator to assist teleoperation," *IEEE/ASME Transactions on Mechatronics*, 2023.
- [23] A. Razjigaev, A. K. Pandey, D. Howard, J. Roberts, and L. Wu, "End-to-end design of bespoke, dexterous snake-like surgical robots: A case study with the raven ii," *IEEE Transactions on Robotics*, vol. 38, no. 5, pp. 2827–2840, 2022.
- [24] D. A. Troncoso, J. A. Robles-Linares, M. Russo, M. A. Elbanna, S. Wild, X. Dong, A. Mohammad, J. Kell, A. D. Norton, and D. Axinte, "A continuum robot for remote applications: From industrial to medical surgery with slender continuum robots," *IEEE Robotics & Automation Magazine*, vol. 30, no. 3, pp. 94–105, 2022.
- [25] Y.-J. Kim, S. Cheng, S. Kim, and K. Iagnemma, "A stiffness-adjustable hyperredundant manipulator using a variable neutral-line mechanism for minimally invasive surgery," *IEEE transactions on robotics*, vol. 30, no. 2, pp. 382–395, 2013.
- [26] J. Hu, T. Liu, H. Zeng, M. X. Chua, J. Katupitiya, and L. Wu, "Static modeling of a class of stiffness-adjustable snake-like robots with gravity compensation," *Robotics*, vol. 12, no. 1, p. 2, 2022.
- [27] D. S. Huang, J. Hu, L. Guo, Y. Sun, and L. Wu, "A static model for a stiffness-adjustable snake-like robot," in *2021 IEEE/RSJ International Conference on Intelligent Robots and Systems (IROS)*. IEEE, 2021, pp. 2956–2961.
- [28] S. Jadhav, M. R. A. Majit, B. Shih, J. P. Schulze, and M. T. Tolley, "Variable stiffness devices using fiber jamming for application in soft robotics and wearable haptics," *Soft Robotics*, vol. 9, no. 1, pp. 173–186, 2022.
- [29] E. Amanov, T.-D. Nguyen, and J. Burgner-Kahrs, "Tendon-driven continuum robots with extensible sections—a model-based evaluation of path-following motions," *The International Journal of Robotics Research*, vol. 40, no. 1, pp. 7–23, 2021.
- [30] S. Frieler, S. Misra, and V. K. Venkiteswaran, "Selectively tunable joints with variable stiffness for a magnetically-steerable 6-dof manipulator," *IEEE Transactions on Medical Robotics and Bionics*, 2024.